
Figures and figure supplements

SNAP25 disease mutations change the energy landscape for synaptic exocytosis due to aberrant SNARE interactions

Anna Kádková, Jacqueline Murach and Maiken Østergaard *et al.*

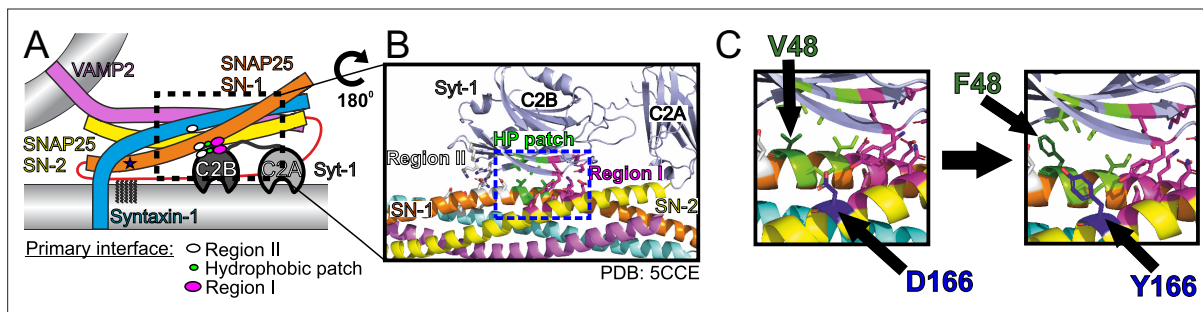


Figure 1. Localization of three pathogenic mutations in SNAP25. **(A)** Schematic of the neuronal SNARE complex interacting with C2B domain of synaptotagmin-1 (Syt1; not to scale) via the primary interface. Position of the I67N mutation in the first SNARE domain of SNAP25 is depicted by an asterisk. **(B)** Interaction site of the C2B domain of Syt1 and SNAP25. Syt1 interacts with SNAP25 both electrostatically (regions I and II) and within the hydrophobic patch (HP patch) (Zhou *et al.*, 2015). **(C)** Position of the disease-linked mutations V48F (hydrophobic patch) and D166Y (region I) in the SNARE complex.

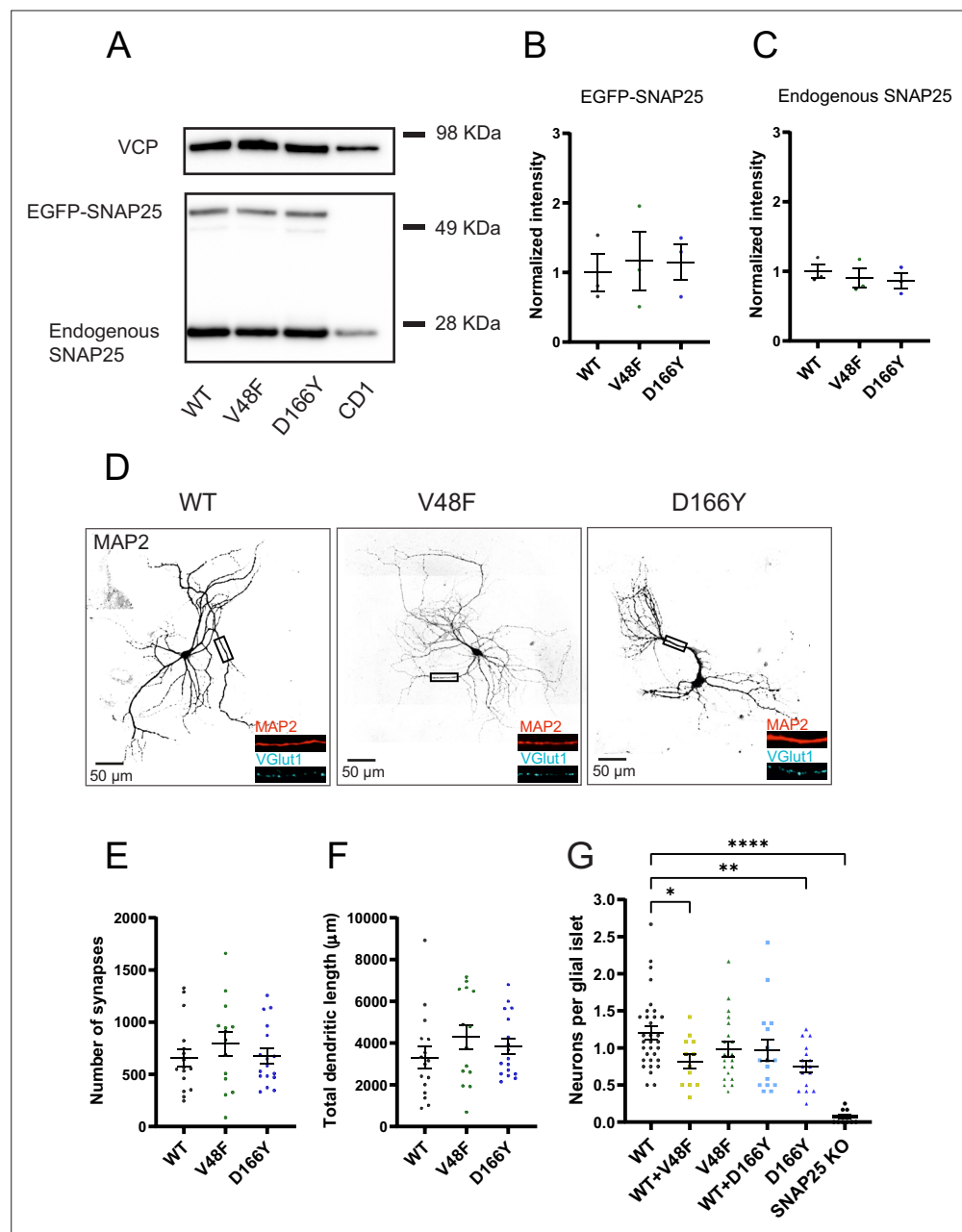


Figure 2. Pathogenic SNAP25 mutations compromise neuronal viability, but not synaptogenesis. **(A)** SNAP25b V48F and D166Y mutations are similarly expressed as the wildtype (WT) SNAP25b protein. EGFP-SNAP25b was overexpressed in neurons from CD1 (WT) mice; both endogenous and overexpressed SNAP25 are shown. Valosin-containing protein (VCP) was used as loading control. Quantification of EGFP-SNAP25b **(B)** and endogenous SNAP25 **(C)** from Western blots (as in A). Displayed are the intensity of EGFP-SNAP25b or endogenous SNAP25 bands, divided by the intensity of VCP bands, normalized to the WT situation ($n = 3$ independent experiments). The expression level of mutants was indistinguishable from expressed WT protein (analysis of variance, ANOVA). **(D)** Representative images of control (WT) and mutant (V48F, D166Y) hippocampal neurons stained by dendritic (MAP2) and synaptic (VGlut1) markers. Displayed is MAP2 staining, representing the cell morphology, in inserts MAP2 staining is depicted in red and VGlut1 staining in cyan. The scale bar represents 50 μ m. **(E)** Number of synapses per neuron in WT and mutant cells. **(F)** Total dendritic length of WT and mutant neurons. **(G)** Cell viability represented as the number of neurons per glial island. **** $p < 0.0001$, ** $p < 0.01$, * $p < 0.05$, Brown-Forsythe ANOVA test with Dunnett's multiple comparisons test.

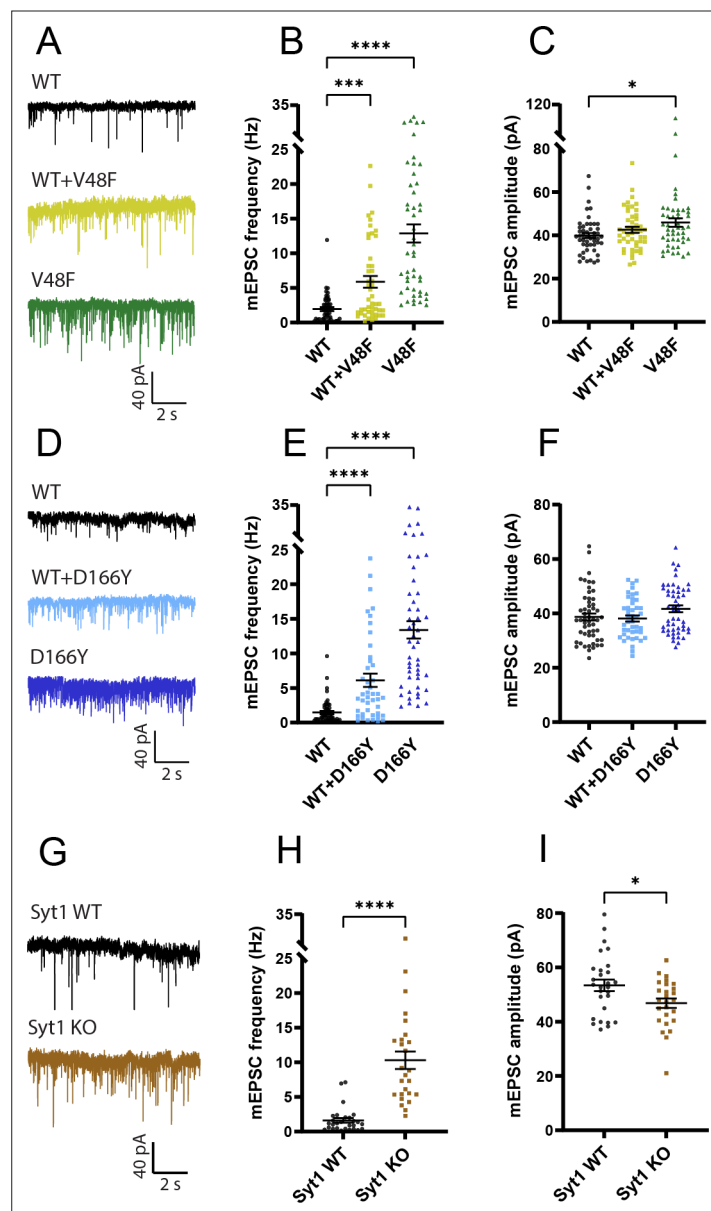


Figure 3. V48F and D166Y mutations increase mEPSC frequency. (A, D, G) Example traces of mEPSC release for wildtype (WT), mutant, and 1:1 co-expression of WT and mutant SNAP25b, or (G) Syt1 WT and knockout (KO). (B, E) The mEPSC frequencies were increased in both V48F and D166Y mutants and co-expressed conditions (V48F: $n = 49, 47, 48$ for WT, co-expressed, and mutant conditions, respectively; D166Y: $n = 54, 43, 50$). **** $p < 0.0001$, *** $p < 0.001$, Brown–Forsythe analysis of variance (ANOVA) test with Dunnett’s multiple comparisons test. (C, F) mEPSC amplitudes were on average increased by the V48F and D166Y mutations; this was significant for the V48F. * $p < 0.05$, ANOVA with Dunnett’s multiple comparison test. (H, I) Syt1 WT and KO data (Syt1: $n = 28, 26$ for the WT and KO condition). The mEPSC frequencies and amplitudes were increased and decreased in the KO, respectively. **** $p < 0.0001$, Welch’s t -test, * $p < 0.05$, unpaired t -test.

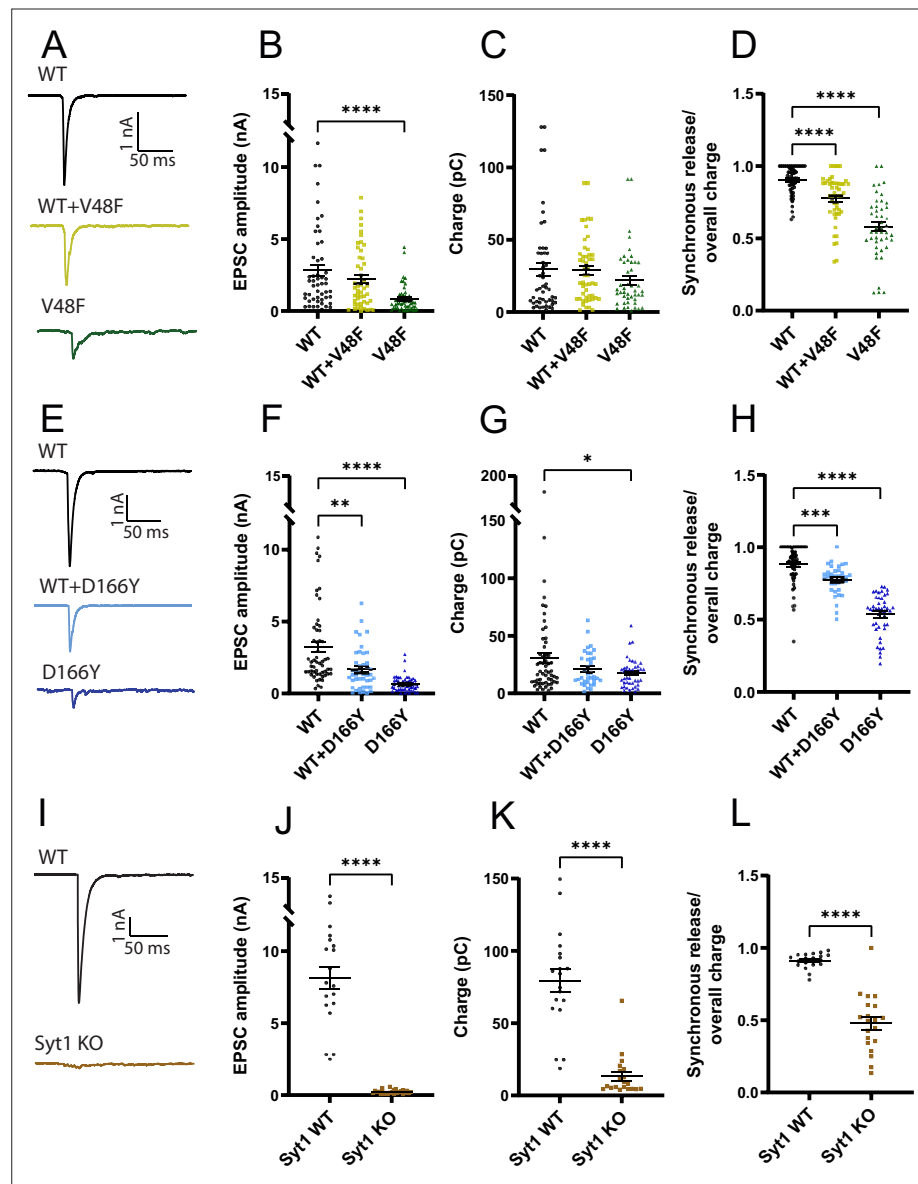


Figure 4. V48F and D166Y mutations reduce the amplitude of the eEPSC. (A, E, I) Example evoked excitatory postsynaptic currents (eEPSC) for wildtype (WT), SNAP25b mutants, and co-expressed WT/mutants, or (I) Syt1 WT and knockout (KO). (B, F, J) eEPSC amplitude was decreased by both SNAP25b mutations (V48F: $n = 50, 50, 45$ for WT, co-expressed, and mutant conditions, respectively; D166Y: $n = 56, 35, 44$) and by Syt1 KO (Syt1: $n = 19, 26$ for the WT and KO condition). SNAP25b mutations: **** $p < 0.0001$, ** $p < 0.01$, Brown–Forsythe analysis of variance (ANOVA) test with Dunnett’s multiple comparisons test; Syt1: **** $p < 0.0001$, Welch’s t -test. (C, G, K) Overall evoked charge after a single depolarization (V48F: $n = 50, 45, 50$ for WT, mutant, and co-expressed conditions, respectively; D166Y: $56, 44, 35$; Syt1: $19, 20$ for WT and KO). SNAP25b: * $p < 0.05$, Brown–Forsythe ANOVA with Dunnett’s multiple comparison test; Syt1: **** $p < 0.0001$, Welch’s t -test. (D, H, L) Fractional contribution of the synchronous release component to the overall charge (V48F: $n = 50, 50, 45$ for WT, co-expressed, and mutant conditions, respectively; D166Y: $56, 35, 44$; Syt1: $19, 20$ for WT and KO). SNAP25b: **** $p < 0.0001$, *** $p < 0.001$, Brown–Forsythe ANOVA (V48F) or standard ANOVA (D166Y) with Dunnett’s multiple comparisons test; Syt1: **** $p < 0.0001$, Welch’s t -test.

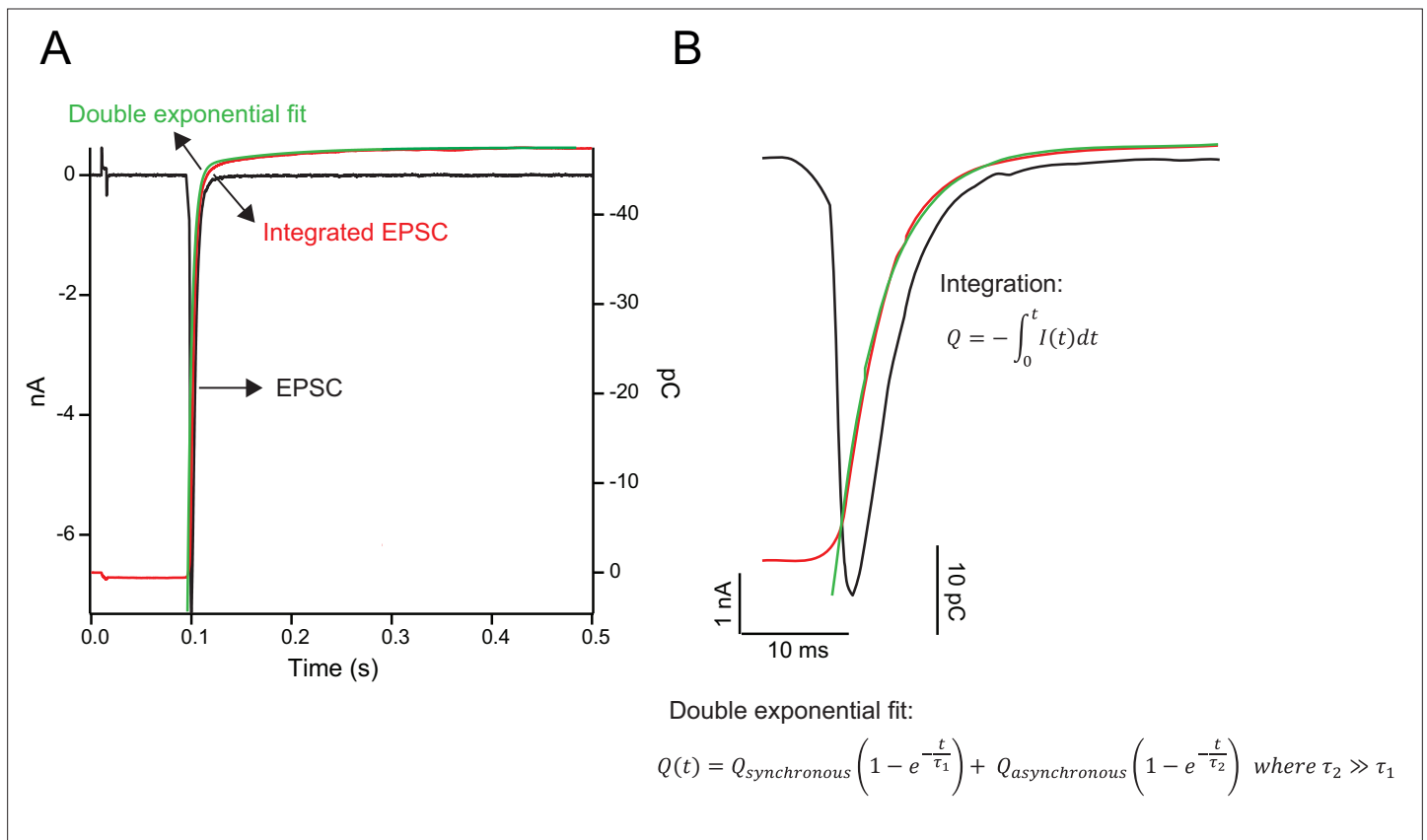


Figure 4—figure supplement 1. Kinetic parameters of evoked EPSCs. **(A)** eEPSC (black trace), and integrated eEPSC (after multiplication with -1 , red trace) with double exponential fit (green trace). **(B)** Zoom-in of eEPSC (black trace), and integrated eEPSC (after multiplication with -1 , red trace) with double exponential fit (green trace). Equations for integration and double exponential function used for fit are given.

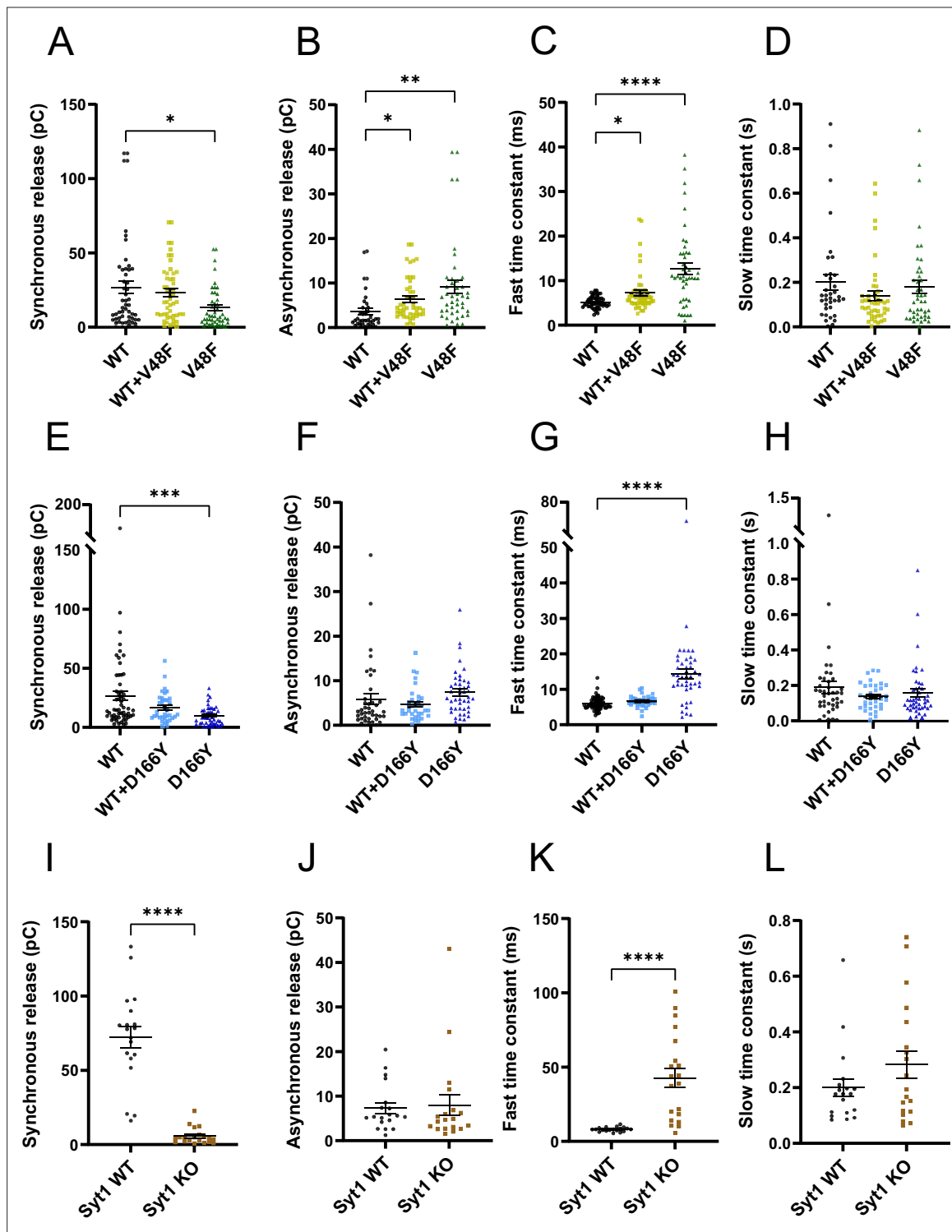


Figure 4—figure supplement 2. Kinetic parameters of eEPSCs. (A, E, I) Synchronous release components (A), V48F: $n = 50, 50, 45$ for wildtype (WT), co-expressed, and mutant conditions, respectively; E, D166Y: $n = 56, 35, 44$; I, Syt1: 19, 20 for WT and knockout [KO]. (A) $*p < 0.05$, Welch's analysis of variance (ANOVA) with Dunnett's multiple comparison test, (E) $***p < 0.001$, Brown–Forsythe ANOVA with Dunnett's multiple comparison test, (I) $****p < 0.0001$, Welch's unpaired t-test. (B, F, J) Asynchronous release components. (B) $**p < 0.01$; $*p < 0.05$, Brown–Forsythe ANOVA with Dunnett's multiple comparison test. (C, G, K) Fast time constants. (C): $****p < 0.0001$; $**p < 0.01$, Brown–Forsythe ANOVA with Dunnett's multiple comparison test, (G): $****p < 0.0001$, Brown–Forsythe ANOVA with Dunnett's multiple comparison test, (K): $****p < 0.0001$, Welch's unpaired t-test. (D, H, L) Slow time constants. Source Data containing quantitative data are found in the Source Data files for **Figure 4**.

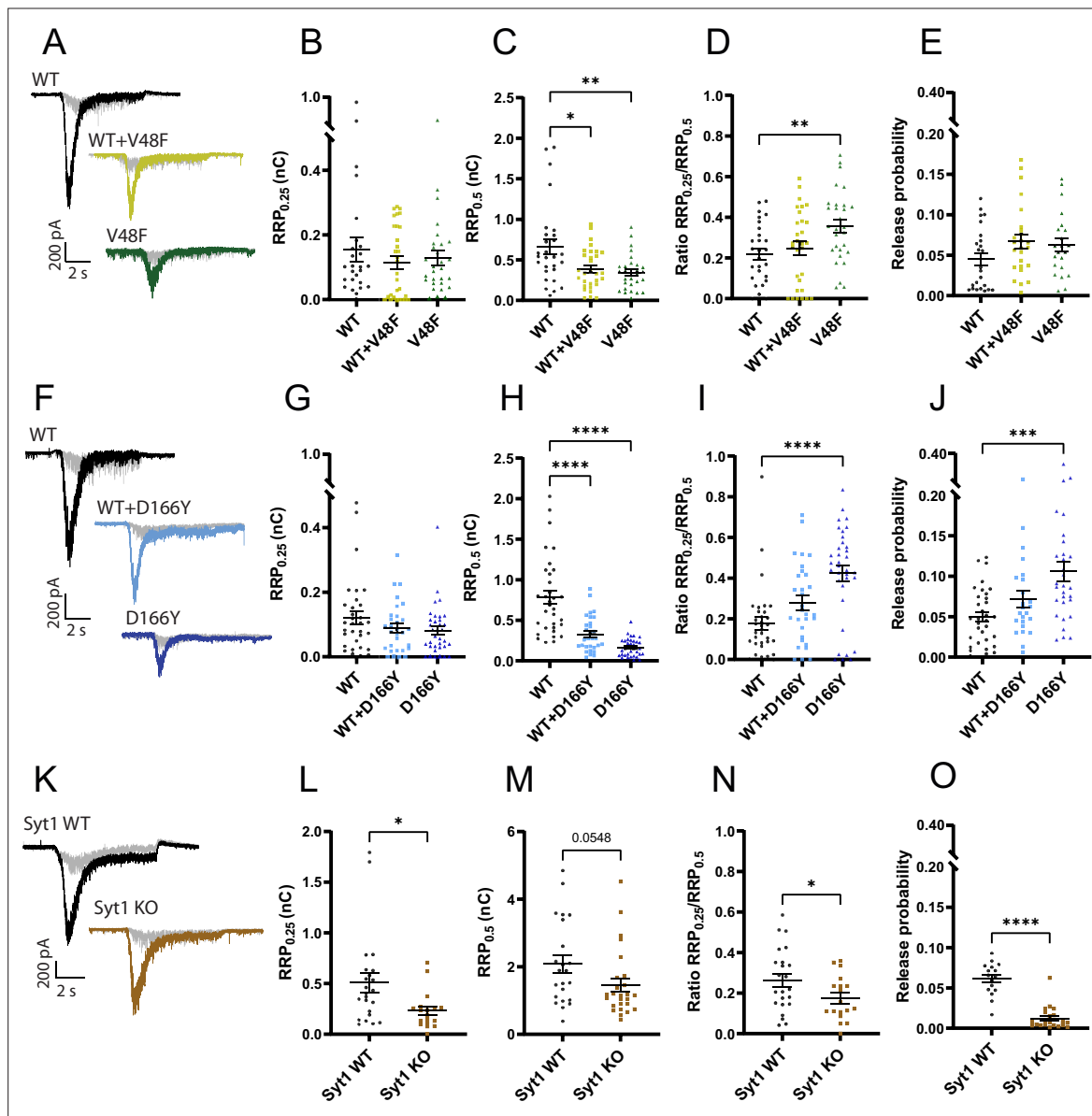


Figure 5. The apparent energy barrier for vesicle fusion is lowered by V48F and D166Y, but not by removing Syt1. (A, F, K) Example traces for the wildtype (WT), mutant, and co-expressed condition. Each cell was stimulated by 0.25 M (in gray) and 0.5 M sucrose (in black or color). (B, G, L) The charge released by 0.25 M sucrose (V48F: $n = 28, 30, 29$ for WT, co-expressed, and mutant conditions, respectively; D166Y: $n = 33, 30, 35$; Syt1: $n = 23, 18$ for WT and knockout [KO]). Syt1: $p < 0.05$, Welch's t -test. (C, H, M) The charge released by 0.5 M sucrose (V48F: $n = 28, 30, 29$ for WT, co-expressed, and mutant conditions, respectively; D166Y: $n = 33, 30, 35$; Syt1: $n = 23, 26$ for WT and KO). SNAP25b: **** $p < 0.0001$, ** $p < 0.01$, * $p < 0.05$, Brown-Forsythe analysis of variance (ANOVA) with Dunnett's multiple comparisons test; Syt1: $p = 0.0548$, unpaired t -test. (D, I, N) The ratio of 0.25 and 0.5 M sucrose pool (V48F: $n = 28, 30, 29$ for WT, co-expressed, and mutant conditions, respectively; D166Y: $n = 33, 30, 35$; Syt1: $n = 23, 18$ for WT and KO). SNAP25b: **** $p < 0.0001$, ** $p < 0.01$, ANOVA with Dunnett's multiple comparisons test; Syt1: * $p < 0.05$, unpaired t -test. (E, J, O) Release probability calculated by dividing the charge of an eEPSC with the 0.5 M sucrose pool (V48F: $n = 24, 25, 22$ for WT, co-expressed, and mutant conditions, respectively; D166Y: $n = 33, 24, 30$; Syt1: $n = 16, 21$ for WT and KO). SNAP25b: *** $p < 0.001$, ANOVA with Dunnett's multiple comparisons test; Syt1: **** $p < 0.0001$, unpaired t -test.

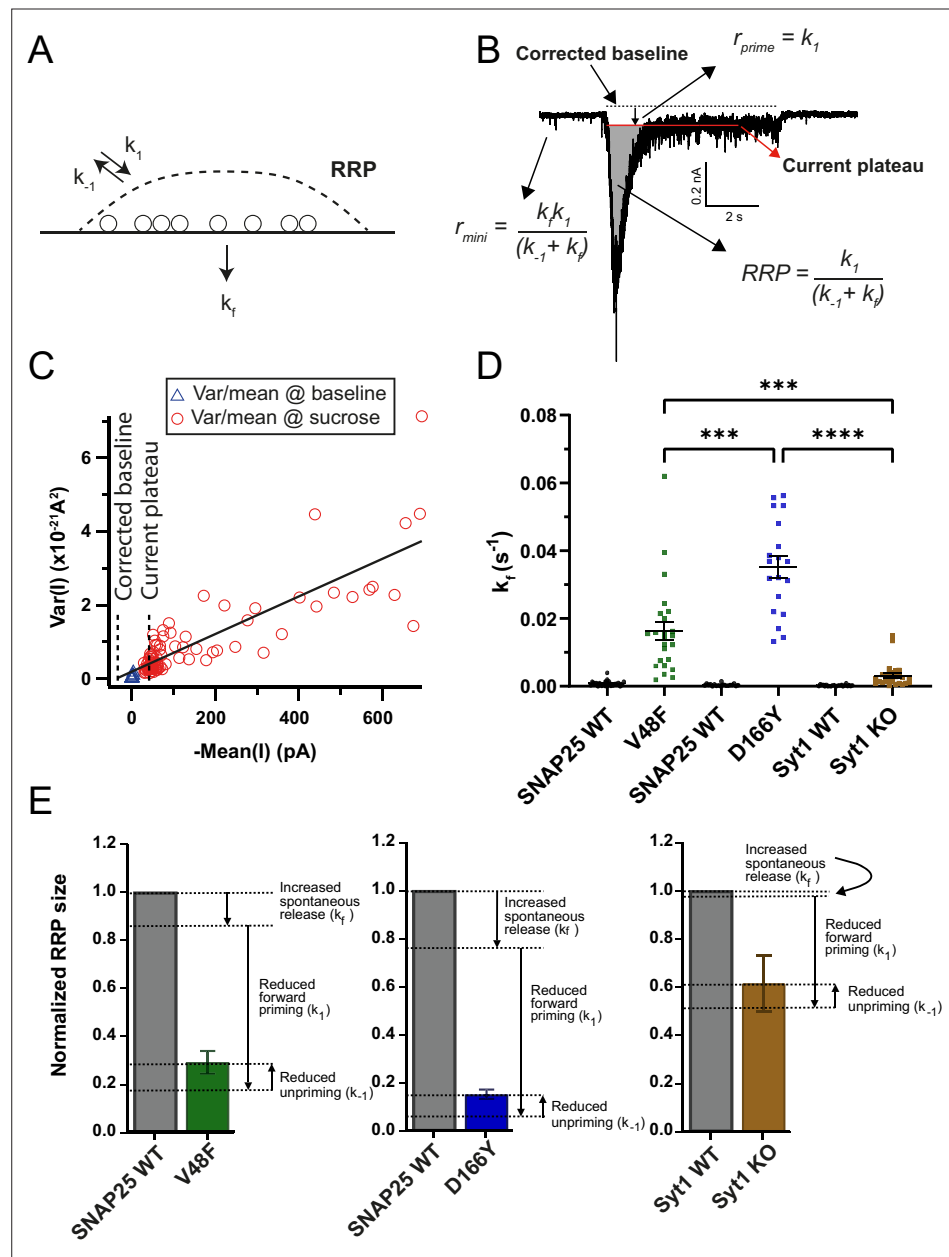


Figure 6. Dissection of the readily releasable pool (RRP) reduction in V48F and D166Y mutations. **(A)** One-pool model of the RRP. k_1 is the rate of priming (units vesicles/s), k_{-1} is the rate of depriming (s^{-1}), and k_f is the rate of fusion (s^{-1}). **(B)** Estimation of the three parameters from the response to 0.5 M sucrose and a measurement of the spontaneous release rate. **(C)** Variance-mean analysis in 50-ms intervals during the sucrose application allows determination of the corrected baseline by back-extrapolation of a regression line to the variance of the baseline. **(D)** Normalized mEPSC frequency (k_f) for V48F, D166Y, and Syt1 knockout (KO) (V48F: $n = 23, 24$ for wildtype [WT] and mutant conditions, respectively; D166Y: $n = 19, 19$; Syt1: $n = 23, 26$). Brown–Forsythe analysis of variance (ANOVA) test with Dunnett’s multiple comparison test, testing the three mutant conditions against each other. **** $p < 0.0001$, *** $p < 0.001$. **(E)** Normalized RRP size for WT and mutant conditions, with indications of the effect of the mutant-induced changes in k_1 , k_{-1} , and k_f on the RRP size.

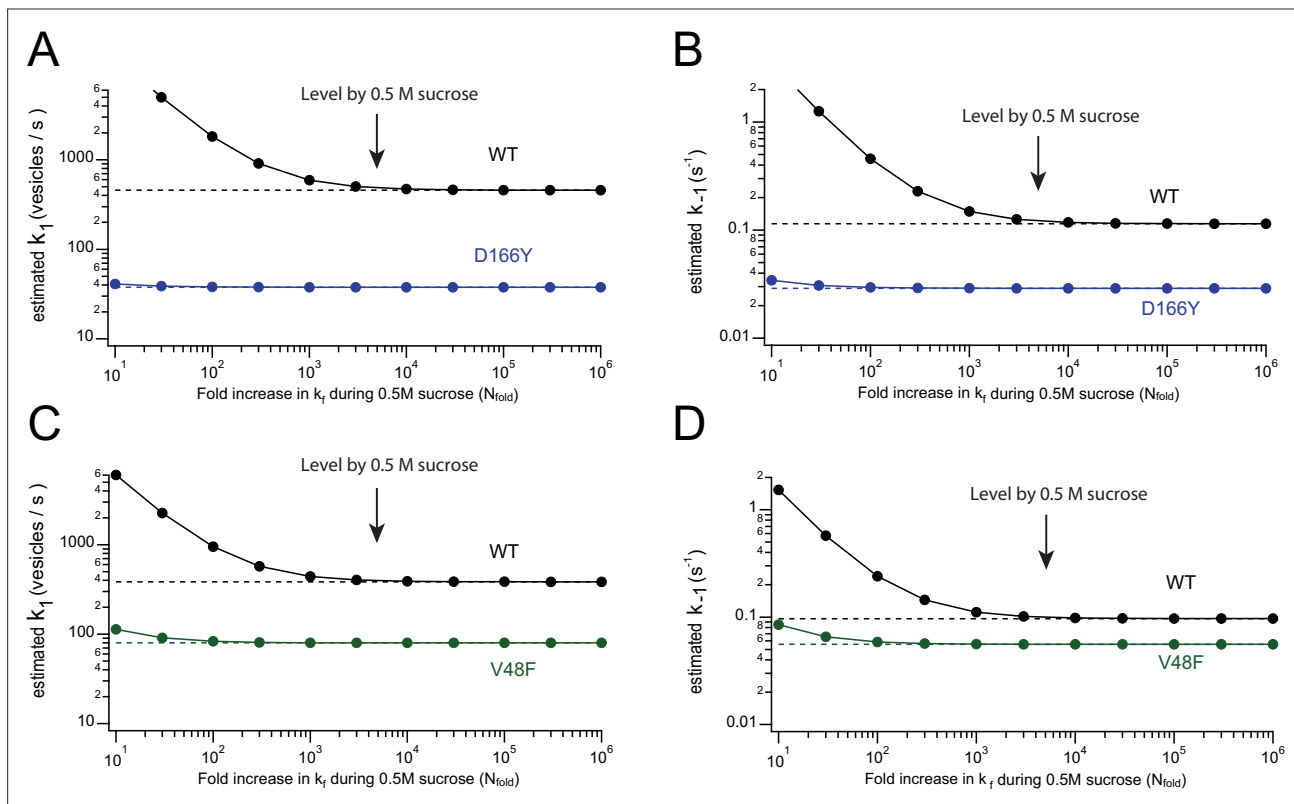


Figure 6—figure supplement 1. Effect of sucrose stimulation on estimates of k_1 and k_{-1} . The figure shows the effect of the fold-increase in fusion rate (N) induced by sucrose (abscissa) on the estimates of k_1 (A, C) or k_{-1} (B, D) using **Equations 3 and 4**, **Equation 5b** and the values estimated for D166Y (A, B), V48F (C, D), and wildtype (WT) (**Table 1**). Previous data showed that 0.5 M sucrose increases the fusion rate by a factor ~ 5000 (Schotten et al., 2015). The plots show that the estimates in **Table 1** are not strongly affected by small changes in the effect of sucrose upon k_f .

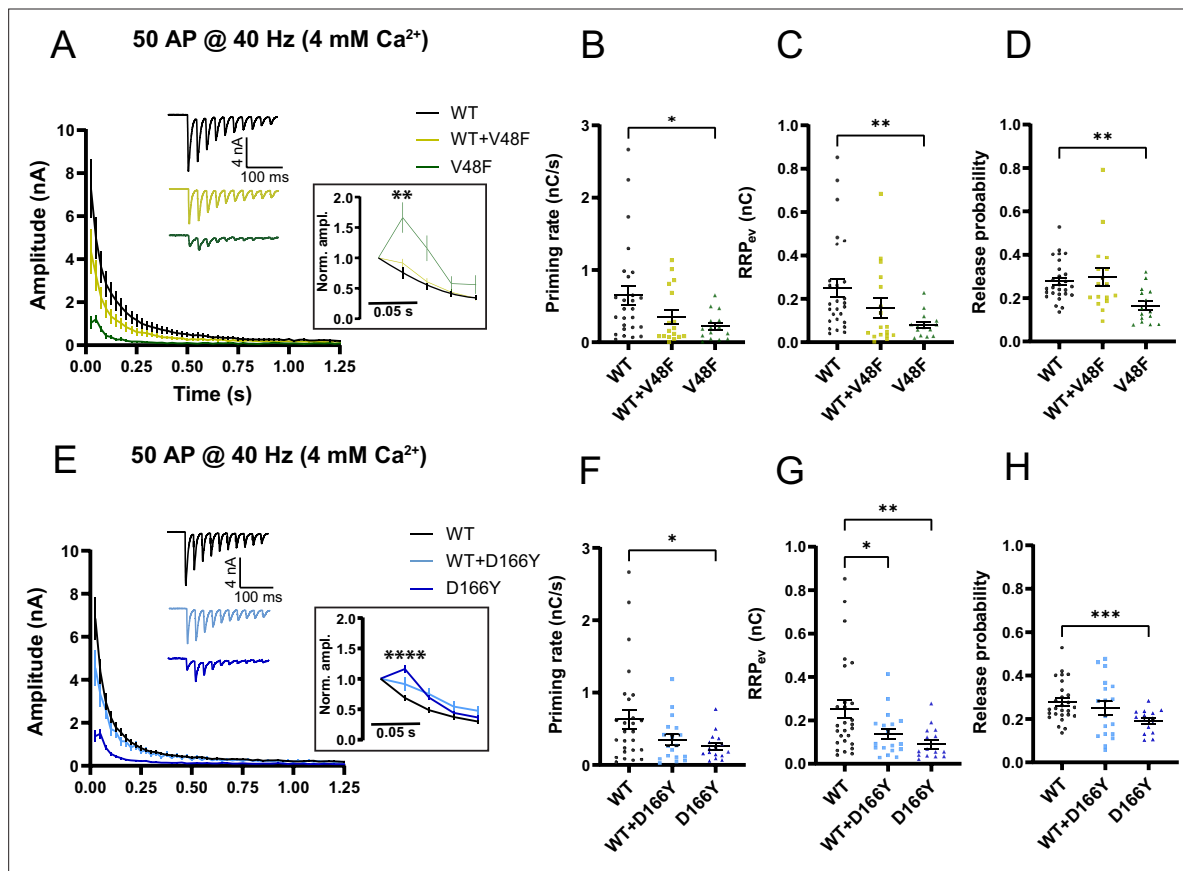


Figure 7. SNAP25 V48F and D166Y mutations change short-term plasticity toward facilitation. (**A, E**) eEPSCs in response to 50 APs at 40 Hz recorded in 4 mM extracellular Ca^{2+} (V48F: 27, 17, 15 for wildtype [WT], co-expressed, and mutant conditions, respectively; D166Y: 27, 18, 16). Insets: Normalized eEPSC amplitudes demonstrating facilitation of mutant conditions. ****p < 0.0001; **p < 0.01, Brown–Forsythe analysis of variance (ANOVA) with Dunnett’s multiple comparison test. (**B, F**) Priming rate calculated as the slope of a linear fit to the cumulative evoked charges during the last part of stimulation (V48F: 27, 17, 15 for WT, co-expressed, and mutant conditions, respectively; D166Y: 27, 18, 16). *p < 0.05, ANOVA (V48F) or Brown–Forsythe ANOVA (D166Y) with Dunnett’s multiple comparisons test. (**C, G**) Readily releasable pool (RRP) calculated by back-extrapolation of a linear fit to the cumulative evoked charges during the last part of stimulation (V48F: 27, 17, 15 for WT, co-expressed, and mutant conditions, respectively; D166Y: 27, 18, 16). **p < 0.01, *p < 0.05, ANOVA (V48F), or Brown–Forsythe ANOVA (D166Y) with Dunnett’s multiple comparisons test. (**D, H**) Release probability calculated as the charge of the first evoked response divided by the RRP obtained by back-extrapolation (V48F: 27, 17, 15 for WT, co-expressed, and mutant conditions, respectively; D166Y: 27, 18, 16). ***p < 0.001; **p < 0.01, ANOVA (V48F), or Brown–Forsythe ANOVA (D166Y) with Dunnett’s multiple comparisons test.

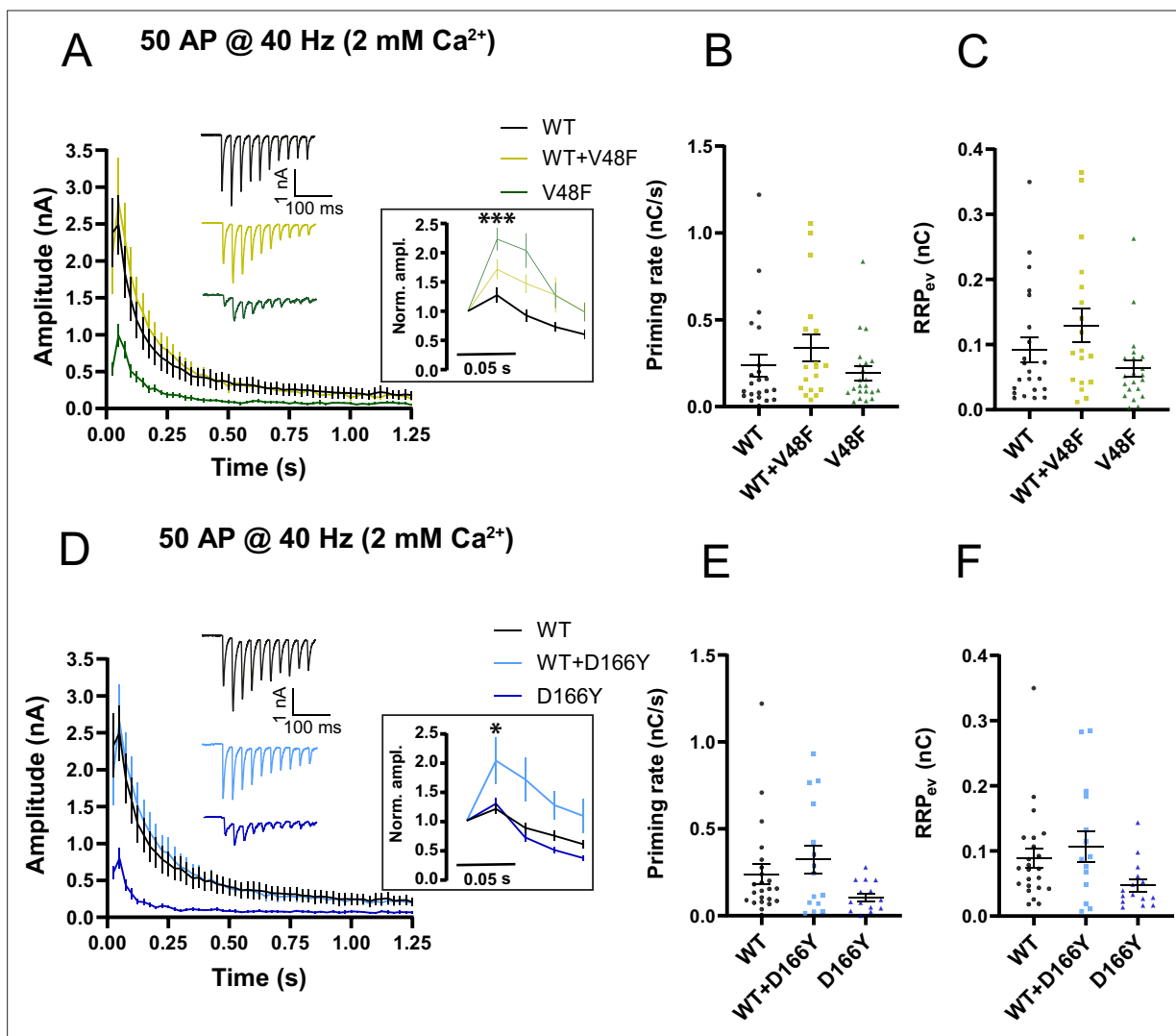


Figure 7—figure supplement 1. Train stimulations of V48F and D166Y in 2 mM Ca^{2+} . (**A, D**) eEPSCs in response to 50 APs at 40 Hz recorded in 2 mM extracellular Ca^{2+} (V48F: 25, 18, 24 for wildtype [WT], co-expressed, and mutant conditions, respectively; D166Y: 23, 15, 15). Inserts: Normalized eEPSC amplitudes of first ten stimulations. *p < 0.05, ***p < 0.001, one-way analysis of variance (ANOVA) with Dunnett's multiple comparison test. (**B, E**) Priming rate calculated by as the slope of a linear fit to the cumulative evoked charges during the last part of stimulation (V48F: 24, 18, 24 for WT, co-expressed, and mutant conditions, respectively; D166Y: 23, 15, 15). (**C, F**) Readily releasable pool (RRP) calculated by back-extrapolation of a linear fit to the cumulative evoked charges during the last part of stimulation (V48F: 24, 18, 24 for WT, co-expressed, and mutant conditions, respectively; D166Y: 23, 15, 15).

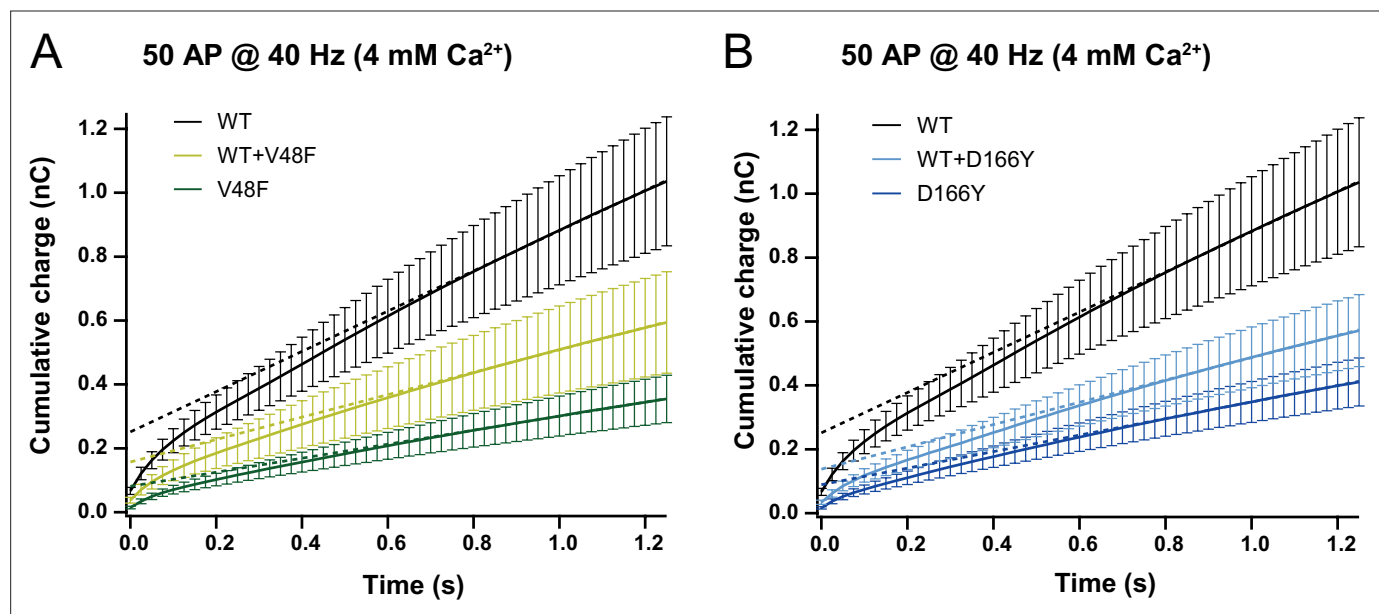


Figure 7—figure supplement 2. Cumulative charges of V48F and D166Y trains in 4 mM Ca^{2+} . (A, B) Cumulative charges obtained by integrating eEPSCs during 40 Hz trains. The slope of the linear part of the curve reports on the priming rate, which is reduced by the mutations. The back-extrapolation of the linear fit to zero time reports on the RRP_{ev} , the part of the readily releasable pool (RRP) which APs draw on, which is also reduced by mutation (V48F: $n = 27, 17, 15$ for wildtype [WT], co-expressed, and mutant conditions, respectively; D166Y: 27, 18, 16).

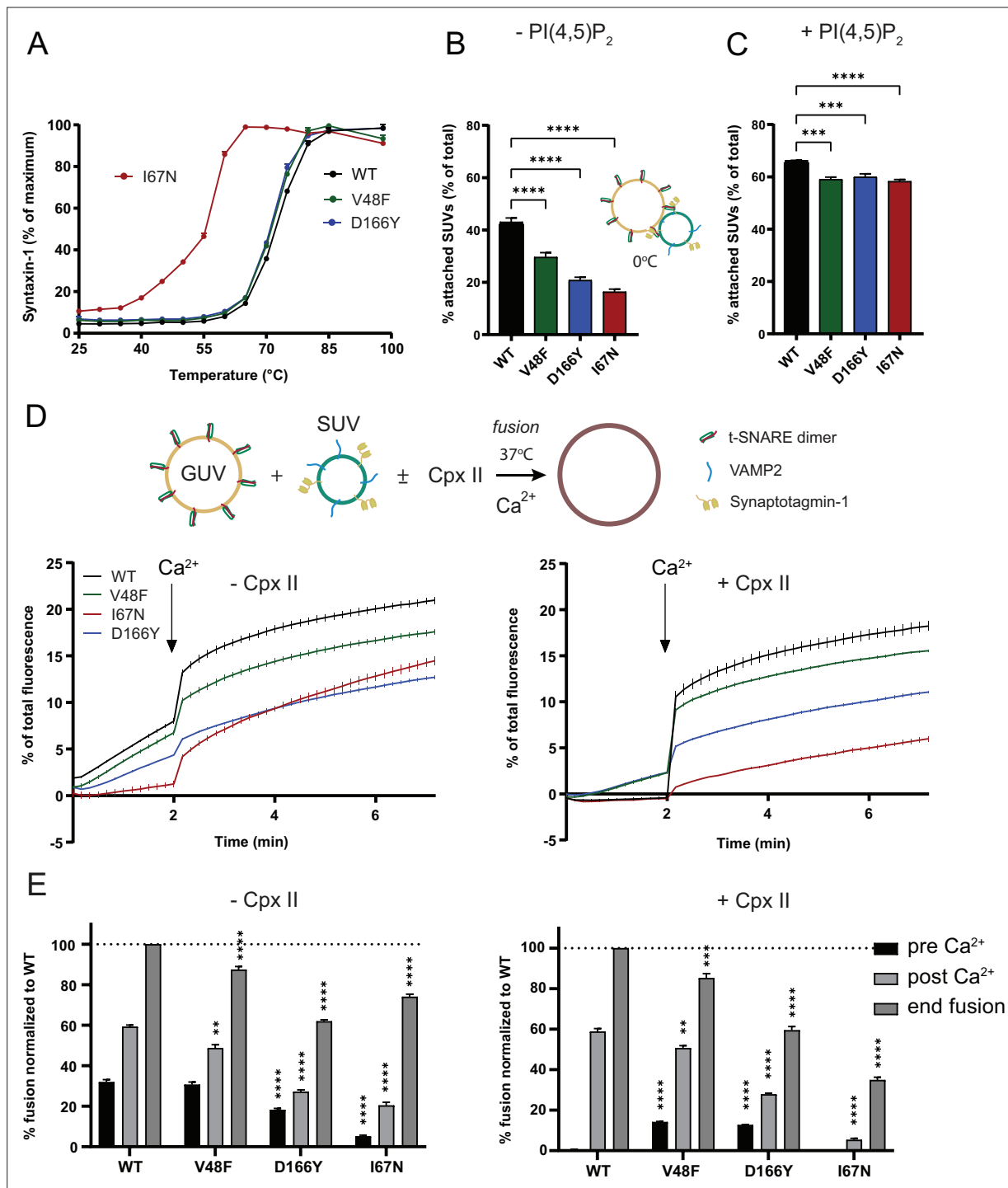


Figure 8. Pathogenic SNAP25 mutations affect synaptotagmin-1 interaction and fusion rates in vitro. **(A)** In the presence of SDS, SNAP25b I67N containing v-/t-SNARE complexes were more sensitive to temperature-dependent dissociation. Shown are mean \pm standard error of the mean (SEM; $n = 3$) for SNARE complexes including SNAP25b wildtype (WT) and the I67N, V48F, and D166Y mutations. **(B, C)** In vitro Syt1/VAMP2 small unilamellar vesicles (SUVs) docking to t-SNARE giant unilamellar vesicles (GUVs) was significantly reduced by SNAP25b V48F, I67N, and D166Y mutants either in absence **(B)** or presence **(C)** of PI(4,5)P₂. Fusion was blocked by performing the assay on ice. **** $p < 0.0001$; *** $p < 0.001$, analysis of variance (ANOVA) with Dunnett's multiple comparison test. **(D, E)** In vitro lipid mixing assays of VAMP/Syt1 SUVs with t-SNARE GUVs containing SNAP25b V48F, I67N, or D166Y mutants showed impaired membrane fusion in the absence (left) or presence (right) of complexin-II. Fusion clamping in the presence of complexin was selectively reduced by V48F and D166Y. Bar diagrams show lipid mixing just before (pre) and after (post) Ca²⁺ addition and at the end of the reaction. Shown is mean \pm SEM ($n = 3$). **** $p < 0.0001$; ** $p < 0.01$, ANOVA with Dunnett's multiple comparisons test, comparing each mutation to the corresponding WT condition.

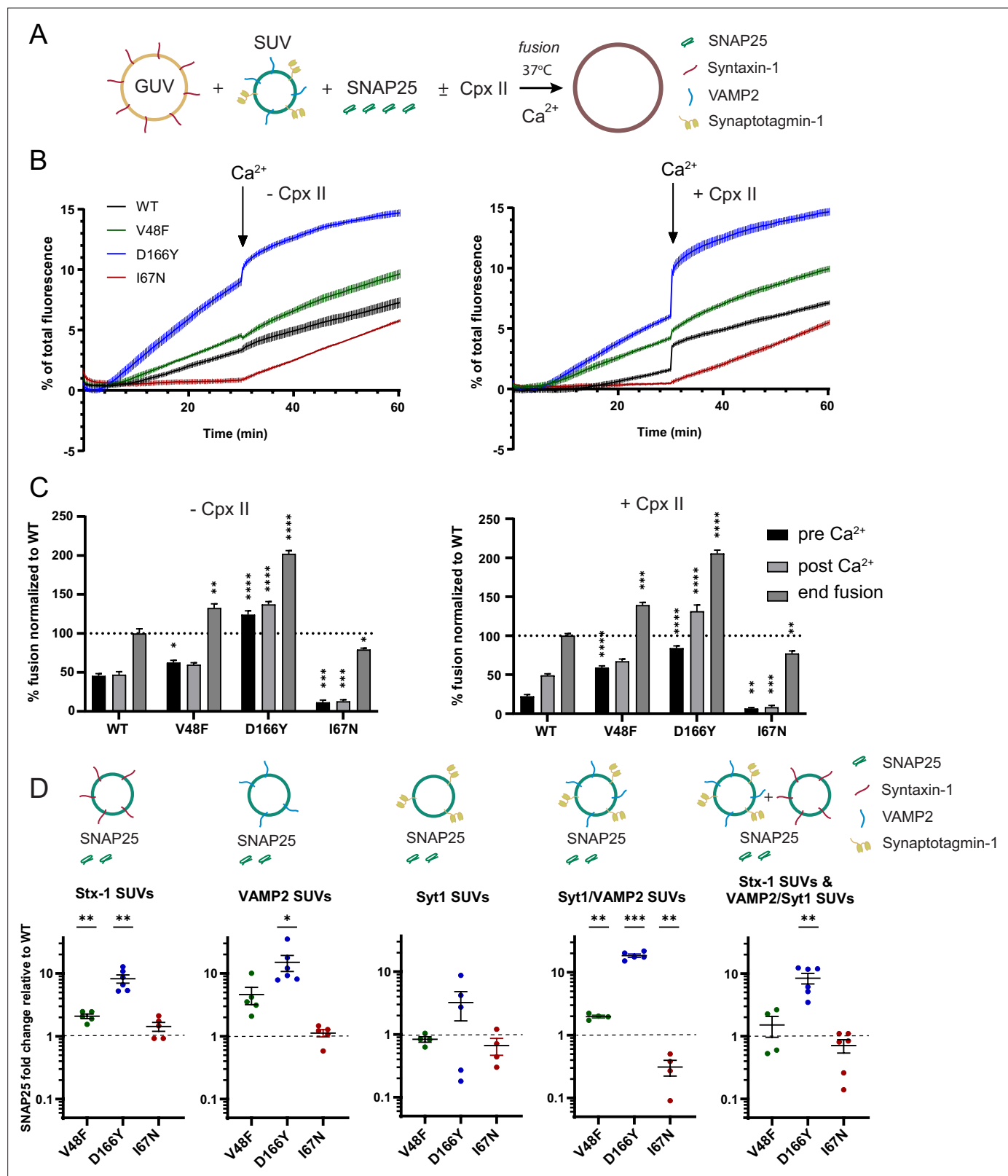


Figure 9. The D166Y mutation increases binding to its SNARE partners. (A–C) In vitro lipid mixing assays of VAMP/Syt1 small unilamellar vesicles (SUVs) with syntaxin-1A giant unilamellar vesicles (GUVs) in the presence of soluble SNAP25b. V48F and D166Y mutants showed impaired fusion clamping in the absence (left) or presence (right) of complexin-II; I67N (red) showed impaired Ca^{2+} -independent and Ca^{2+} -triggered fusion. Bar diagrams show lipid mixing just before (pre) and after (post) Ca^{2+} addition and at the end of the reaction. Mean \pm standard error of the mean (SEM; $n = 3$). **** $p < 0.0001$.

Figure 9 continued on next page

Figure 9 continued

0.0001; *** $p < 0.001$; ** $p < 0.01$; * $p < 0.05$, analysis of variance (ANOVA) with Dunnett's multiple comparisons test, comparing each mutation to the corresponding wildtype (WT) condition. **(D)** SNAP25b D166Y showed enhanced interactions with SUVs carrying reconstituted syntaxin-1A (Stx-1), VAMP2, Syt1/VAMP2, or an SUV mixture containing Syntaxin-1A and VAMP2/Syt1 in co-flotation assays, whereas V48F displayed weaker increases in interactions with SUVs containing syntaxin-1A, or Syt1/VAMP2. Shown is mean \pm SEM on a logarithmic scale. *** $p < 0.001$, ** $p < 0.01$, * $p < 0.05$, two-tailed one-sample t -test comparing to 1.

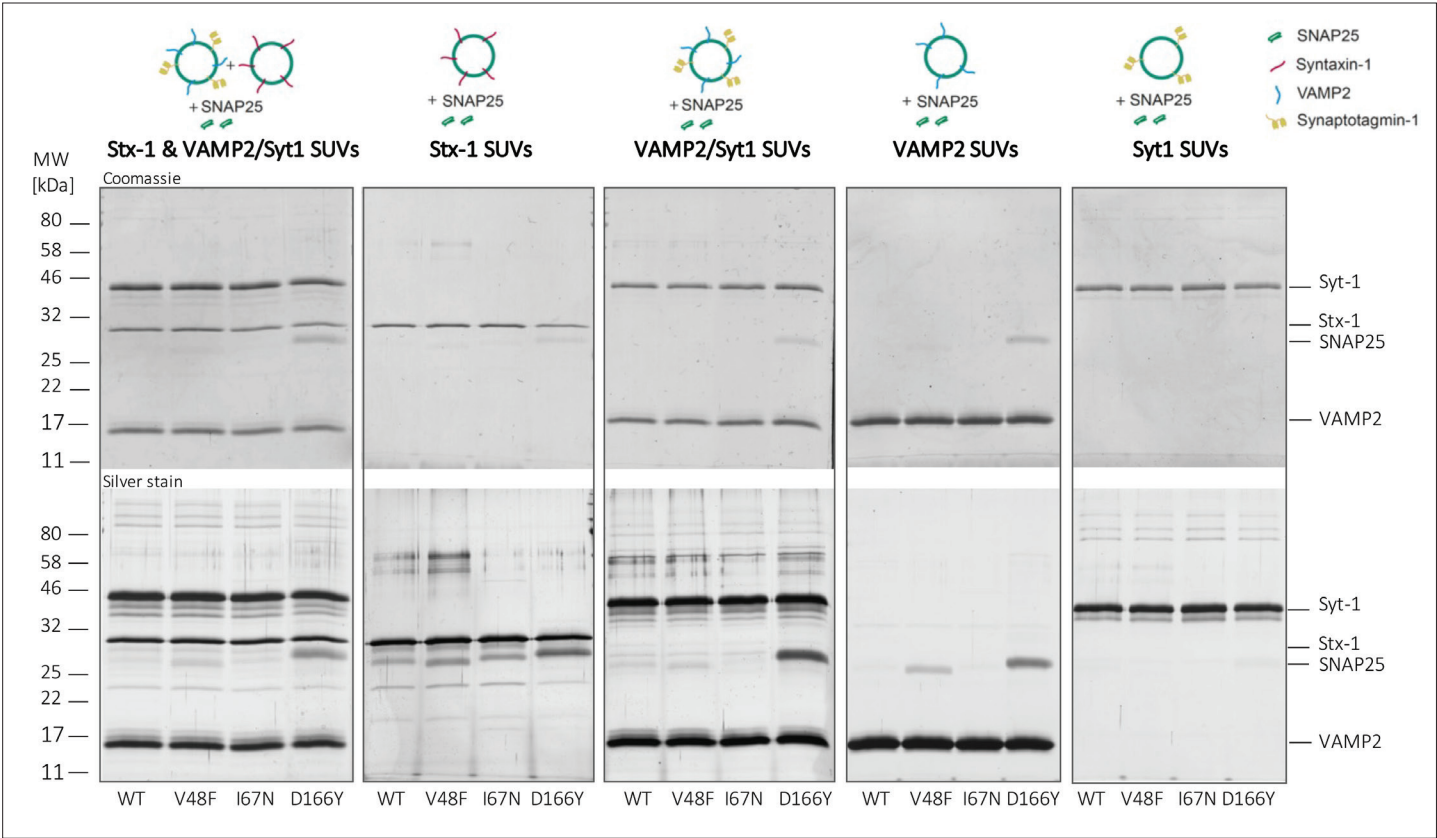


Figure 9—figure supplement 1. Flootation assay. Example Coomassie and silver stained gels demonstrating binding of SNAP25b wildtype (WT) and mutants to different populations of small unilamellar vesicles (SUVs): Syntaxin-1 (Stx-1) and VAMP2/Syt1, Syntaxin-1 (Stx-1), VAMP2/Syt1, VAMP2, or Syt1 SUVs. Note increased binding of D166Y and V48F to most SUV populations, strongest for D166Y (quantified data in **Figure 9D**).

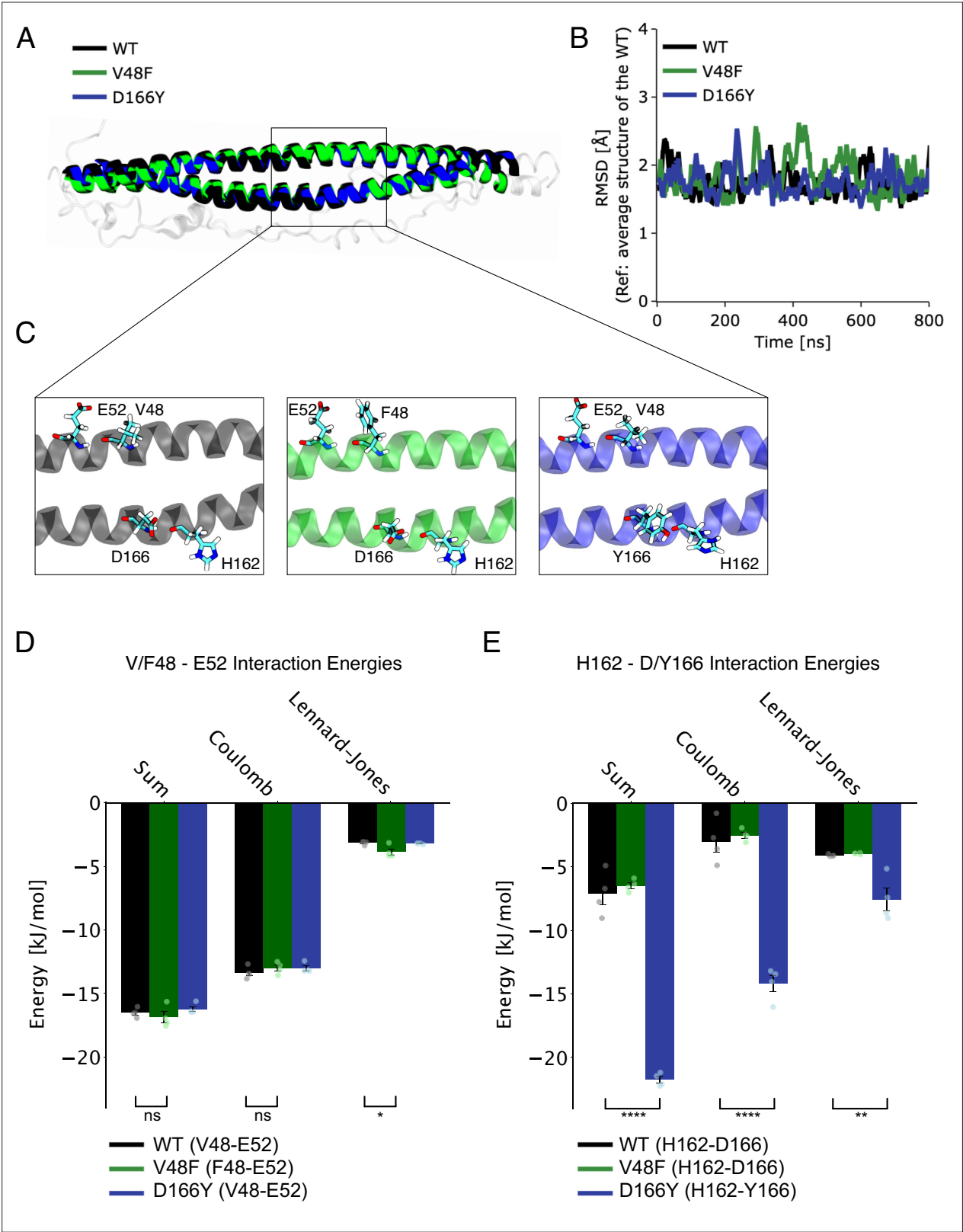


Figure 9—figure supplement 2. Molecular dynamics simulations of mutants. **(A)** Alignment of helices across the three systems (wildtype [WT], V48F, and D166Y) reveals close correspondence. The structures displayed represent the most prevalent configurations from the dominant cluster observed during simulations. **(B)** Stability evaluation (Root Mean Square Deviation, RMSD) of the two helices across the three systems relative to WT's average structure during their simulations. **(C)** A detailed view of the region displaying residue pairs 48–52 and 162–166 on the structures. **(D, E)** Computed

Figure 9—figure supplement 2 continued on next page

Figure 9—figure supplement 2 continued

electrostatic (Coulomb) and van der Waals (Lennard–Jonson, LJ) interactions for residue pairs 48–52 (**D**) and 162–166 (**E**) calculated in 200 ns blocks within the 800 ns trajectory (see Materials and methods). The bar plots represent the means calculated using the block averaging method, while each block's average is depicted as a dot alongside. The error bars capture the standard error of the mean, premised on treating each block as an independent measure (i.e. $n = 4$). Notably, for D166Y (panel E, blue bar), the interaction energy is considerably more negative, indicating a stronger interaction compared to WT. * $p < 0.05$, ** $p < 0.01$, **** $p < 0.0001$, one-way analysis of variance (ANOVA) with Tukey HSD post hoc tests.

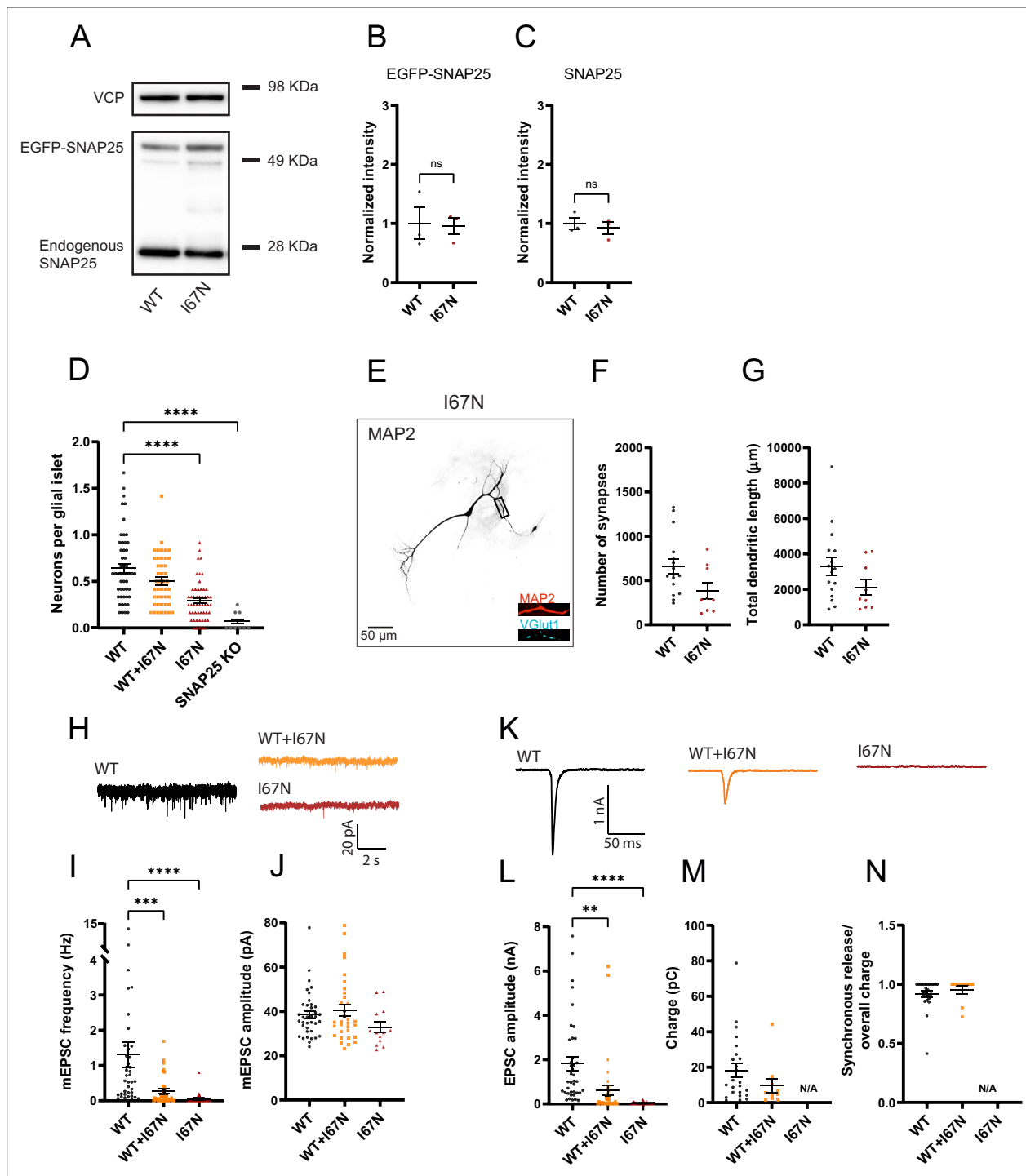


Figure 10. The I67N mutation inhibits spontaneous and evoked release. **(A)** SNAP25b I67N is similarly expressed as the wildtype (WT) SNAP25b protein. EGFP-SNAP25b was overexpressed in neurons from CD1 (WT) mice; both endogenous and overexpressed SNAP25 are shown. Valosin-containing protein (VCP) was used as the loading control. Quantification of EGFP-SNAP25b **(B)** and endogenous SNAP25 **(C)** from Western blots (as in A). Displayed are the intensity of EGFP-SNAP25b or endogenous SNAP25 bands, divided by the intensity of VCP bands, normalized to the WT situation ($n = 3$ independent experiments). The expression level of the I67N mutant was indistinguishable from WT protein (analysis of variance, ANOVA). **(D)** Cell viability represented as the number of neurons per glial islet. **** $p < 0.0001$, Brown–Forsythe ANOVA test with Dunnett’s multiple comparisons test. **(E)** Representative image of mutant (I67N) hippocampal neurons stained for the dendritic marker MAP2 and the synaptic markers VGLut1. Displayed is MAP2 staining, representing the cell morphology, in inserts MAP2 staining is depicted in red and VGLut staining in cyan. The scale bar represents 50 μm . **(F)** Number of synapses per neuron in WT and mutant cells. The WT data are the same as in **Figure 2D, E** because these experiments were carried out in parallel. The difference was tested using ANOVA between all conditions, which was non-significant. **(G)** Total dendritic length of WT and

Figure 10 continued on next page

Figure 10 continued

mutant neurons. **(H)** Example traces of mEPSC release for WT, mutant (I67N), and 1:1 co-expression of WT and SNAP25 mutant. **(I)** The mini frequency was decreased in both I67N mutant and the WT + I67N combination (I67N: $n = 39, 36, 30$ for WT, co-expressed and mutant). **** $p < 0.0001$, *** $p < 0.001$, Kruskal–Wallis with Dunn’s multiple comparisons. **(J)** mEPSC amplitudes were unchanged by the I67N mutation. **(K)** Example evoked excitatory postsynaptic currents (eEPSC) for WT, mutant (I67N), and co-expressed WT and mutant. **(L)** eEPSC amplitude was decreased by the I67N mutations (I67N: $n = 39, 37, 30$ for WT, co-expressed and mutant conditions, respectively). SNAP25b mutations: **** $p < 0.0001$, ** $p < 0.01$, Brown–Forsythe ANOVA test with Dunnett’s multiple comparisons test. **(M)** Overall evoked charge after a single depolarization (I67N: 24, 10, 0 for WT, co-expressed and mutant conditions, respectively). **(N)** Fractional contribution of the synchronous release component to the overall charge (I67N: 24, 10, 0 for WT, co-expressed, and mutant conditions, respectively). Source Data containing quantitative data are found in the Source Data files for **Figures 2–4**.

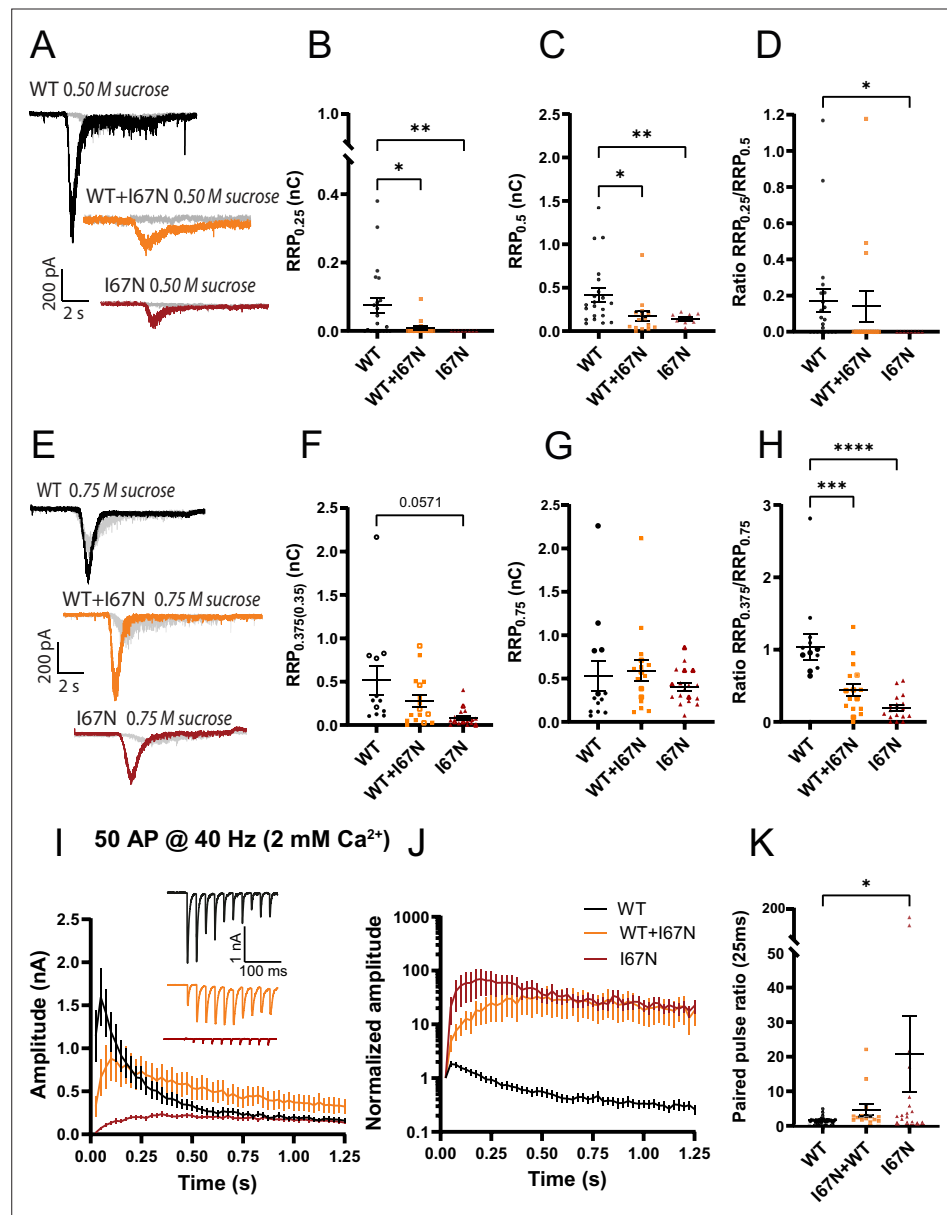


Figure 11. The I67N mutation has normal readily releasable pool (RRP) size, but increased energy barrier for fusion. (A, E) Example traces for the wildtype (WT), mutant, and co-expressed condition. Each cell was stimulated by 0.25 M (A, in gray) and 0.5 M sucrose (A, in color) or 0.375 M sucrose (E, in gray) and 0.75 M (E, in color). The charge released by 0.25 M sucrose (B, I67N: $n = 21, 15, 8$ for WT, co-expressed, and mutant conditions, respectively) or 0.375 M sucrose (F, I67N: $n = 12, 16, 18$; a few cells were stimulated with 0.35 M sucrose – shown with open symbols). (B) ** $p < 0.01$; * $p < 0.05$, Kruskal–Wallis test with Dunn’s multiple comparison test; (F) $p = 0.0339$ Brown–Forsythe analysis of variance (ANOVA) test; Dunn’s multiple comparison test, $p = 0.0571$. The charge released by 0.5 M sucrose (C, I67N: $n = 21, 15, 8$ for WT, co-expressed, and mutant conditions, respectively), or 0.75 M sucrose (G, I67N: $n = 13, 16, 18$). (C) ** $p < 0.01$, * $p < 0.05$, Brown–Forsythe ANOVA with Dunn’s multiple comparisons test. The ratio of the 0.25 and 0.5 M sucrose pool (D, I67N: $n = 21, 15, 8$ for WT, co-expressed, and mutant conditions, respectively), or the ratio of 0.375 and 0.75 M sucrose pool (H, $n = 13, 16, 18$). (D) * $p < 0.05$, Kruskal–Wallis test with Dunn’s multiple comparisons test. (H) **** $p < 0.0001$; *** $p < 0.001$, ANOVA with Dunn’s multiple comparisons test. (I) eEPSCs in response to 50 APs at 40 Hz recorded in 2 mM extracellular Ca²⁺ (I67N: $n = 23, 16, 20$ for WT, co-expressed, and mutant conditions, respectively). Inserts: Normalized eEPSC amplitudes demonstrating facilitation of mutant conditions. (J) Normalized eEPSC amplitudes in response to 50 APs at 40 Hz recorded in 2 mM extracellular Ca²⁺. (K) Paired-pulse ratio at interstimulus interval 25 ms (I67N: $n = 24, 14, 17$ for WT, co-expressed, and mutant conditions, respectively). * $p < 0.05$, ANOVA with Dunn’s multiple comparison test. Source Data containing quantitative data are found in the Source Data files for Figures 5 and 7.

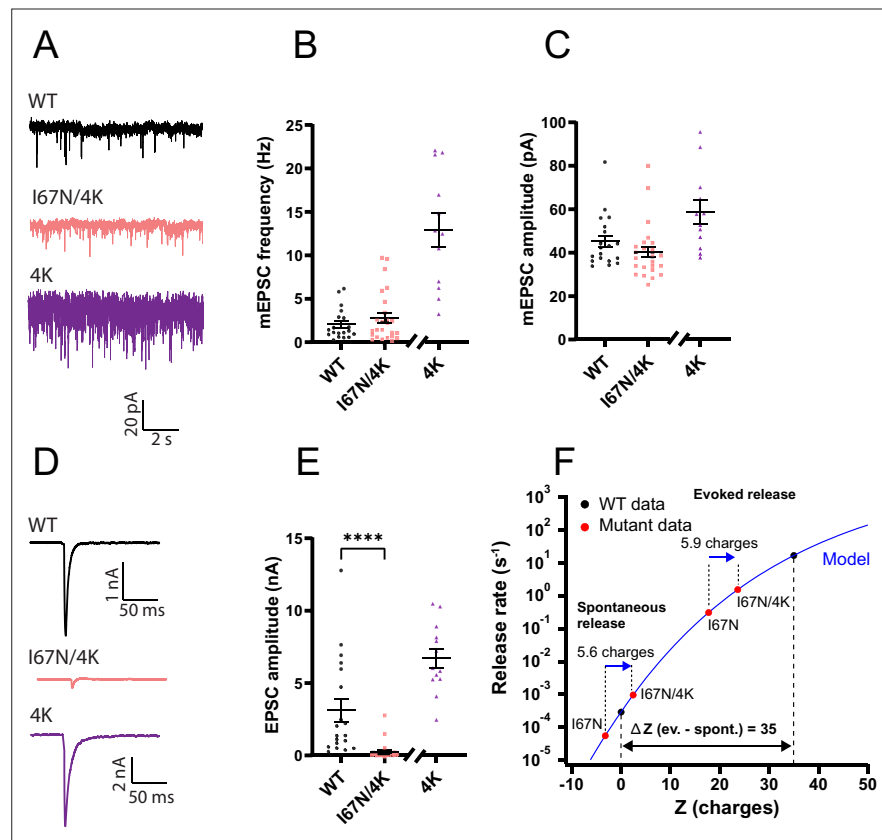


Figure 12. Adding positive surface charges to the SNARE complex partly compensates for the I67N mutation. (A) Example traces of mEPSC release for wildtype (WT), I67N/E183K/S187K/T190K/E194K (I67N/4K) and E183K/S187K/T190K/E194K (4K) SNAP25b. Data from the 4K mutation were obtained in a separate experiment and are shown for comparison, but statistical tests with 4K mutation data were not carried out. (B) The mini frequencies for the WT and I67N/4K are not significantly different; data from the 4K mutation are shown for comparison ($n = 19, 25, 13$ for WT, I67N/4K, and 4K, respectively). (C) Mini amplitudes remain unaffected by I67N/4K mutation. eEPSC examples (D) and amplitudes (E) for WT and I67N/4K; 4K is shown for comparison ($n = 19, 25, 13$ for WT, I67N/4K, and 4K, respectively). **** $p < 0.0001$ Mann–Whitney test. (F) Electrostatic triggering model (blue line; [Ruiter et al., 2019](#)) refitted to WT spontaneous and evoked data points (black points). Fitted parameters: rate 0.00029 s^{-1} at zero (0) charge (Z); fraction $f = 0.030$; the maximum rate was fixed at 6000 s^{-1} . WT (black points), I67N, I67N/4K (red points): means of log-transformed data. The charge values (Z , horizontal axis) for I67N and I67N/4K were found by interpolation in the model; the two spontaneous points (I67N, I67N/4K) are separated by 5.6 charges. For evoked release, rates were found by deconvolution and normalizing to $\text{RRP}_{0.5}$ ([Ruiter et al., 2019](#)). The Z -values for evoked release were found by interpolation in the model; the two mutants (I67N, I67N/4K) are separated by 5.9 charges.

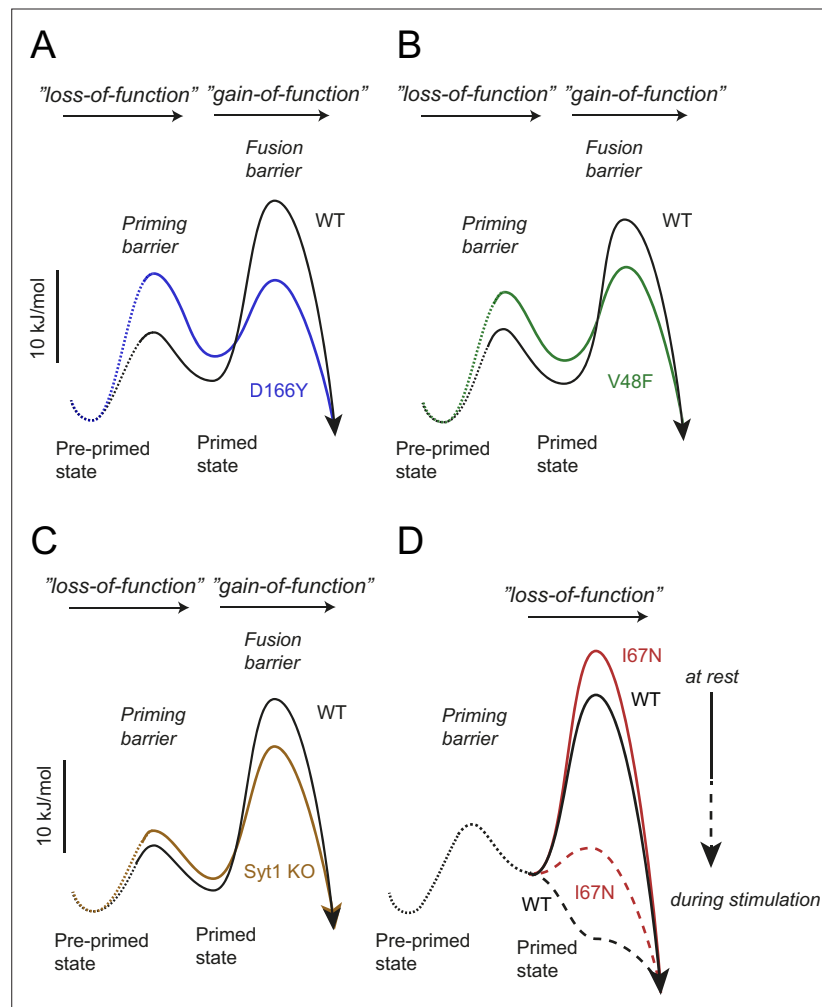


Figure 13. Energy landscapes. The energy landscapes of wildtype (WT) and mutants were calculated as explained in Materials and methods and displayed to scale. Energy landscapes for D166Y (A), V48F (B), and Syt1 knockout (KO) (C) are shown at rest and are characterized by a higher priming barrier ('loss-of-function' phenotype), a destabilized readily releasable pool (RRP), and a lower fusion barrier ('gain-of-function' phenotype). The I67N (D) is characterized by a higher fusion barrier ('loss-of-function' phenotype). The relative increase in the fusion barrier by the I67N mutation is higher during stimulation than at rest. Dotted lines represent energy levels for which less is known.